Structure at 2.3 Å resolution of the cytochrome bc_1 complex from the yeast *Saccharomyces cerevisiae* co-crystallized with an antibody Fv fragment

Carola Hunte*, Juergen Koepke, Christian Lange, Tanja Roßmanith and Hartmut Michel*

Background: The cytochrome bc_1 complex is part of the energy conversion machinery of the respiratory and photosynthetic electron transfer chains. This integral membrane protein complex catalyzes electron transfer from ubiquinol to cytochrome *c*. It couples the electron transfer to the electrogenic translocation of protons across the membrane via a so-called Q cycle mechanism.

Results: The cytochrome bc_1 complex from the yeast *Saccharomyces cerevisiae* was crystallized together with a bound antibody Fv fragment. The structure was determined at 2.3 Å resolution using multiple isomorphous replacement, and refined to a crystallographic R factor of 22.2% (R_{free} = 25.4%). The complex is present as a homodimer. Each 'monomer' of the refined model includes 2178 amino acid residues of subunits COR1, QCR2, COB, CYT1, RIP1, QCR6, QCR7, QCR8 and QCR9 of the cytochrome bc_1 complex and of the polypeptides V_H and V_L of the Fv fragment, the cofactors heme b_H, heme b_L, heme c_1, the [2Fe–2S] cluster and 346 water molecules. The Fv fragment binds to the extrinsic domain of the [2Fe–2S] Rieske protein and is essential for formation of the crystal lattice.

Conclusions: The approach to crystallize membrane proteins as complexes with specific antibody fragments appears to be of general importance. The structure of the yeast cytochrome bc_1 complex reveals in detail the binding sites of the natural substrate coenzyme Q6 and the inhibitor stigmatellin. Buried water molecules close to the binding sites suggest possible pathways for proton uptake and release. A comparison with other cytochrome bc_1 complexes shows features that are specific to yeast.

Address: Max-Planck-Institut für Biophysik, Abt. Molekulare Membranbiologie, Heinrich-Hoffmann-Strasse 7, 60528 Frankfurt, Germany.

*Corresponding authors.
E-mail: michel@mpibp-frankfurt.mpg.de
hunte@mpibp-frankfurt.mpg.de

Key words: coenzyme Q6, matrix processing peptidase, proton transfer, stigmatellin, yeast cytochrome bc_1 complex

Received: **26 January 2000**
Revisions requested: **28 February 2000**
Revisions received: **3 April 2000**
Accepted: **4 April 2000**

Published: **1 June 2000**

Structure 2000, **8**:669–684

0969-2126/00/$ – see front matter

Introduction

The ubiquinol–cytochrome *c* oxidoreductase (cytochrome bc_1 complex, E.C. 1.10.2.2), an oligomeric membrane protein complex, is one of the fundamental components of the respiratory and photosynthetic electron transfer chains. It is present in the inner mitochondrial membrane of eukaryotic organisms as well as in many aerobic and photosynthetic bacteria. The enzyme catalyzes the electron transfer from ubiquinol to cytochrome *c*. This process is coupled with electrogenic translocation of protons across the membrane [1,2]. The complex contains three essential catalytic subunits with characteristic prosthetic groups: cytochrome *b* with two *b*-type hemes; cytochrome c_1 with a *c*-type heme; and the so-called Rieske protein that contains a high-potential [2Fe–2S] cluster. Mitochondrial cytochrome bc_1 complexes possess up to eight additional subunits [3]; seven are known for the complex from the yeast *Saccharomyces cerevisiae* [4,5]. Structure determinations using X-ray crystallography have been reported for mitochondrial bc_1 complexes from beef and chicken heart at ~3 Å resolution [6–8], and for the soluble fragment of the Rieske protein at 1.5 Å resolution [9].

The enzyme uses a Q cycle mechanism, in which proton translocation is achieved by quinone redox reactions at two different binding sites and diffusion of quinones and quinols across the membrane [10,11]. Quinol oxidation at the Q_o site is characterized by the release of two protons to the intermembrane side whereas electron transfer is bifurcated. One electron is transferred via the [2Fe–2S] cluster to cytochrome c_1 and used to reduce cytochrome *c*, the other electron is transferred via heme b_L and heme b_H (where L and H denote low and high potential, respectively) to the Q_i site. At the Q_i site, a bound quinone is reduced to semiquinone and after a second cycle to quinol; the protons required are taken up from the matrix side. The quinol then leaves the binding pocket. The existence of two quinone/quinol-binding sites was confirmed by localization of site-specific inhibitors [6–8,12]. Furthermore, the structures indicated

that the [2Fe–2S]- cluster-carrying domain of the Rieske protein is mobile as it is either not visible or found in different positions in the various crystal forms dependent on Q_o site inhibitor binding or crystal contacts [6–8,12]. An alternating interaction of the extrinsic domain of the Rieske protein with cytochrome *b* and cytochrome c_1 might facilitate the bifurcation of the electron transfer pathway at the Q_o site.

Elucidation of the mechanism of this complex will be greatly improved by a combined approach of X-ray crystallography, spectroscopy and site-directed mutagenesis. Our aim was to crystallize the cytochrome bc_1 complex from the yeast *S. cerevisiae*, in which systems for mutagenesis are already established and the protein is genetically and biochemically well characterized [2,4,13]. It is still very difficult to obtain highly ordered crystals from membrane proteins because a large portion of the protein, namely the hydrophobic membrane spanning region, is covered with detergent and only the polar surfaces of the extrinsic domains can contribute to crystal lattice formation. The approach of co-crystallizing membrane proteins with antibody Fv fragments was developed to increase the probability of crystal formation by enlarging the polar surface of the membrane [14]. This approach was applied successfully to the crystallization of the cytochrome *c* oxidase from *Paracoccus denitrificans* [14,15] and led to the structure determination of this membrane protein [15,16].

We present the structure at 2.3 Å resolution of the cytochrome bc_1 complex from *S. cerevisiae*, co-crystallized with an antibody Fv-fragment. The model of the homodimeric complex consists per monomer of nine subunits of the cytochrome bc_1 complex, its cofactors, two polypeptides of the Fv-fragment and more than 300 water molecules. It also includes the natural substrate coenzyme Q6 (UQ6) bound at the Q_i site. The orientation of the Q_o site inhibitor stigmatellin was unambiguously identified. On the basis of the detailed description of the binding sites, residues are proposed that are important for the formation of enzyme–substrate complexes. The presence of buried water molecules in the vicinity of the binding pockets suggests pathways for proton uptake and release. A comparison with the bovine cytochrome bc_1 complex suggests why the yeast core proteins COR1 and QCR2 do not act as matrix-processing peptidases.

Results and discussion

Fv fragment mediated crystallization

The mitochondrial cytochrome bc_1 complex from *S. cerevisiae* was crystallized as a co-complex with an Fv fragment that was derived from the monoclonal antibody mAB_{18E11}, which recognizes a discontinuous epitope of the Rieske protein. The cytochrome bc_1 complex was purified from crude membrane preparations. The enzymatically active complex had a mean cytochrome b/c_1 ratio of 2.0. It was partly delipidated and the loosely bound small subunit QCR10 was completely removed to obtain homogenous preparations (data not shown). A stable co-complex was formed by mixing this protein with purified $_{18E11}$Fv fragment. Crystallization attempts using the sitting-drop vapour diffusion technique and polyethylene glycol (PEG) 4000 as precipitant resulted in crystals after 2–3 weeks. Whereas the pure cytochrome bc_1 complex alone produced very thin crystalline plates that could not be tested for X-ray diffraction, the co-complex yielded compact crystals with a size of $0.2 \times 0.3 \times 0.3$ mm^3. Microseeding shortened the time period that is needed to obtain large, mature crystals to between one and three days. The size of the crystals increased to a side length of 0.6–1.0 mm.

Structure determination

The crystals belong to space group C2 with unit-cell dimensions of a = 214.5 Å, b = 163.9 Å, c = 147.3 Å and $\beta = 117.5^o$. One monomer is present in the crystallographic asymmetric unit. X-ray data were collected using synchrotron radiation at wavelengths close to 1 Å (Table 1). The crystals diffract X-rays up to 2.2 Å resolution. They are highly radiation-sensitive because data collection can only be performed at 4°C. High-resolution data sets were obtained by merging data from several crystals.

Structure determination was initially attempted by the method of molecular replacement. The 2.5 Å and 2.3 Å resolution data sets (Table 1) were used employing the bovine as well as the chicken cytochrome bc_1 complexes (Protein Data Bank [PDB] entries 1QRC [6] and 3BCC [7]) as search models. Although rotational and translational searches resulted in specific solutions, electron-density maps calculated with phases derived from various search models did not show yeast-specific features, and no density for the co-crystallized Fv fragment appeared. Consequently, the structure was solved by the method of multiple isomorphous replacement (MIR) using data sets of six heavy-atom derivatives (Tables 1 and 2). The structure was refined to a crystallographic R factor of 22.2% (R_{free} 25.4 %) at 2.3 Å resolution (Table 3). An example for the quality of the final electron-density map is shown in Figure 1, (e.g. well defined electron density for solvent molecules close to heme b_L appeared).

Overall structure

An overall view of the structure of the yeast cytochrome bc_1 complex is given in Figure 2a. The complex is an intertwined homodimer as it is known from the homologous bovine and chicken complexes [6–8], and an $_{18E11}$Fv fragment is bound to each Rieske protein. The model includes all nine protein subunits of the cytochrome bc_1 complex that were present in the protein preparation: COR1, QCR2, COB, CYT1, RIP1, QCR6, QCR7, QCR8, QCR9 and heavy (V_H) and light (V_L) chain of the $_{18E11}$Fv fragment (Table 4). The model consists of 2178 residues and

Table 1

Summary of data collection, data statistics and MIR phasing*.

Data set	Native 1	Native 2	pCMB†	pCMS‡	TAMM§	$HgCl_2$	AuCl	K_3IrCl_6
Synchrotron	DORIS	ESRF	ESRF	ESRF	ESRF	DORIS	ESRF	ESRF
Beamline	X11	ID14/3	ID14/3	ID14/3	ID14/3	BW6	ID14/3	BM14
Detector	mar345	marCCD	marCCD	marCCD	marCCD	marCCD	marCCD	CCD
Wavelength (Å)	0.9057	0.931	1.008	1.008	1.008	0.990	1.008	1.105
Resolution (Å)	2.5	2.3	3.5	3.2	3.2	3.5	3.2	3.2
R_{sym} (%)#	11.1	6.5	4.1	7.5	8.4	6.7	7.5	7.8
Measured reflections	424,516	1,057,968	172,685	246,830	220,860	342,201	91,168	613,096
Multiplicity	3.04	6.27	1.87	3.86	3.54	6.71	2.02	4.29
Completeness (%)	90.7	84.9	85	89.3	86.5	93.5	62.5	98.3
R_{merge} (%)¶			18.0	20.3	20.9	17.4	19.3	9.4
Sites/monomer			12	11	11	8	8	10
R_{Cullis} (%)¥			75	75	90	75	89	94
Phasing power**			1.3	1.2	0.9	1.3	0.7	0.3

*All diffraction data were collected on synchrotron radiation sources at 4°C. †p-Chloromercuribenzoic acid. ‡p-Chloromercuribenzenesulphonic acid. §Tetrakis-acetoxy-mercury-methane. #$R_{sym} = \Sigma_{hkl}\Sigma_i|I_i - \langle I\rangle|/\Sigma\langle I\rangle$, I_i is the intensity of the ith measurement of reflection hkl and $\langle I\rangle$ is the average intensity of a reflection. ¶$R_{merge} = \Sigma_{hkl}||F_P| - |F_{PH}||/\Sigma_{hkl}|F_P|$, F_P and F_{PH} are the structure factors for the native protein and the heavy atom derivatives. ¥$R_{cullis} = \Sigma_{hkl}(|F_{PH}(obs)| - |F_{PH}(calc)|)/\Sigma_{hkl}(|F_{PH}(obs)| - F_P(obs)|)$, summation is done using centric reflections only. **Phasing power = F_H/E, where F_H is the heavy-atom structure factor and E is the lack of closure error.

is of very good completeness for most subunits with only a few missing residues at the presumably flexible C termini of V_H, V_L, QCR9 and at the N terminus of QCR6. In addition, the cofactors heme b_L, heme b_H, heme c_1 and the [2Fe–2S] cluster (Figure 2b) as well as the Q_o site inhibitor stigmatellin, endogenous UQ6 and 346 water molecules are included. Furthermore, electron density in the transmembrane region indicates the presence of phospholipid molecules for which assignment is in progress.

The $_{18E11}$Fv fragment binds to the surface of the extrinsic domain of the Rieske protein (Figure 2c). The binding is mediated mainly by polar interactions between the complementarity determining region 3 (CDR3: Glu100, Tyr102 and Asp110) as well as CDR1 (Tyr33) of the V_H polypeptide and a discontinuous epitope of the Rieske protein. The latter is formed by an α-helical peptide (Ile126 to Asn130) and Ala144 of this subunit. The Fv fragment is essential for the crystal packing as it forms crystal contacts along the (0.5a + c),b plane with all dimers being packed in the same orientation. The *strep*-tag, an affinity purification peptide at the C terminus of V_H, interacts with the C terminus of subunit QCR7 of the second monomer. Interdimeric crystal contacts are also formed along the a,b plane between COR1, Rieske protein and QCR6. A third group of crystal contacts exists at the interface between the two monomers along the twofold crystallographic axis. The bound Fv fragment allows a spacious and rigid crystal packing with the dimers sufficiently detached to avoid interference of the belt-like detergent micelle (which surrounds the transmembrane region of the complex) with the crystal packing. This example demonstrates the usefulness of the approach to obtain well-ordered crystals of membrane proteins by co-crystallization with antibody Fv fragments first shown for the cytochrome *c* oxidase [14–16].

Each monomer of the dimeric complex consists of a central core of 12 transmembrane helices: eight transmembrane helices of cytochrome *b*, one membrane-anchoring helix each of the Rieske protein and cytochrome c_1 as well as a single transmembrane helix each of subunit QCR8 and QCR9 (Figure 3). The helices of cytochrome *b* are packed in two bundles: a five-helix bundle close to the dimer interface, and a three-helix bundle at the periphery. On the matrix side, subunit QCR7 and the two core proteins are attached to this membrane-spanning block. On the intermembrane side the redox centre carrying domains of cytochrome c_1 and Rieske protein as well as subunit QCR6 are located. Subunit QCR10 is not present in the protein preparations used. Subunit 11 of the bovine heart

Table 2

MIR phase determination.

Resolution (Å)	7.14	5.14	4.56	3.78	3.23	2.82	Total
Reflections	2620	7116	11936	18030	25293	31726	66721
Figure of merit	0.8047	0.8136	0.7155	0.5862	0.3833	0.2151	0.5556

Table 3

Summary of the crystallographic data of the refined model.

Unit cell	
a, b, c (Å)	214.473, 163.921, 147.276
β (°)	117.502
V (Å^3)	4592617
Space group	C2
Complexes per asymmetric unit	1
Subunits	9 + 2 (Fv)
Amino acids	1944 + 234
Vm (Å^3/Da)	4.92
Solvent content (%)	74.98
Water molecules	346
B_{Wilson}*	52.1
Highest resolution	2.3
Unique reflections	168,517
Completeness (%)	
Overall	84.9
Highest resolution shell	73.8
Atoms refined	17,781
R_{merge} (%)	6.09
R_{factor} (%, $F > 0\,\sigma(F)$)	22.2
R_{free} (%)†	25.4

*B_{Wilson} is an average temperature factor for the crystal. †The R_{free} is calculated from 2.5% of the measured unique data, that were not optimized during refinement.

Figure 1

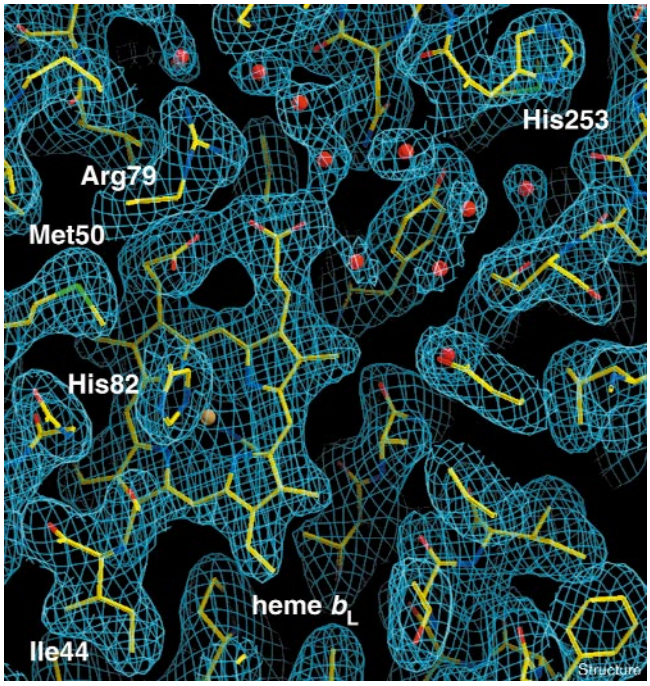

A representative part of the final $2F_o–F_c$ electron-density map showing electron density for heme b_L, neighbouring amino acid residues and water molecules close to one propionate group of the heme; the final model is superimposed. Protein model and heme are shown as stick drawings, water molecules and the heme iron in ball representation. The map is contoured at 1.0σ; atoms are shown in standard colours. The figure was prepared using the program O [46].

complex (Table 4), homologous to QCR10, forms a transmembrane helix that is bound on the outside of the complex to the helices of Rieske protein and subunit 10 (the QCR9 homologue) [8]. Removal of the polypeptide did not affect enzymatic activity [3], but it might be of importance for the correct assembly of the complex [5]. Because of the similar overall structure of the yeast compared with the bovine and chicken complex especially in the transmembrane region (see below), we assume that this subunit will be associated with the complex in the same way. The relative positions of the four different redox centres of the cytochrome bc_1 complex are shown in Figure 2b. The orientations of the heme groups and the distances between the iron positions are in accordance with those known from bovine and chicken cytochrome bc_1 complexes [6–8].

Comparison between the yeast and bovine cytochrome bc_1 complex structures

The general shape, dimension and topology of the yeast cytochrome bc_1 complex and of the complexes from bovine and chicken heart [6–8] are similar. Homologous subunits determined by comparison of the structures are listed in Table 4. They are in agreement with previous assignments of corresponding subunits based on sequence homology, biochemical and genetic studies [4,5]. Superimposition of the structures showed that the fold of the different subunits resembles that of the homologous subunits of the bovine cytochrome bc_1 complex. The presence of secondary structure elements is often very similar, but the exact position, length and conformation of connecting loops varies. An alignment of the structures of the corresponding subunits of the yeast and bovine complexes (PDB code 1BE3 [8]) was performed and the root mean square deviations (rmsd; positional rmsd of superimposed C_α atoms) are listed in Table 4. The structural conservation is most pronounced for the catalytic subunits cytochrome *b*, cytochrome c_1 and the extrinsic domain of the Rieske protein (1.0, 1.5 and 1.0 Å rmsd, respectively). Likewise, sequence alignment showed highest similarity for these subunits (Table 4). For the N-terminal and the transmembrane region of the Rieske protein (residues 31–81) a higher degree of structural variation was found (3 Å rmsd), which coincides with a lower sequence homology. Subunits QCR6 and QCR8 showed an rmsd of 1.5 and 1.8 Å, respectively. Even higher deviations were found for subunits COR1, QCR9 and QCR7 (2.0, 2.4 and 2.5 Å rmsd, respectively). The highest structural difference between homologous subunits was found for QCR2 (2.6 Å rmsd). The summation of various structural differences of this large molecule, together with the presence of 234 additional residues introduced by the $_{18E11}$Fv fragment might have been responsible for the failure in solving the structure by molecular replacement.

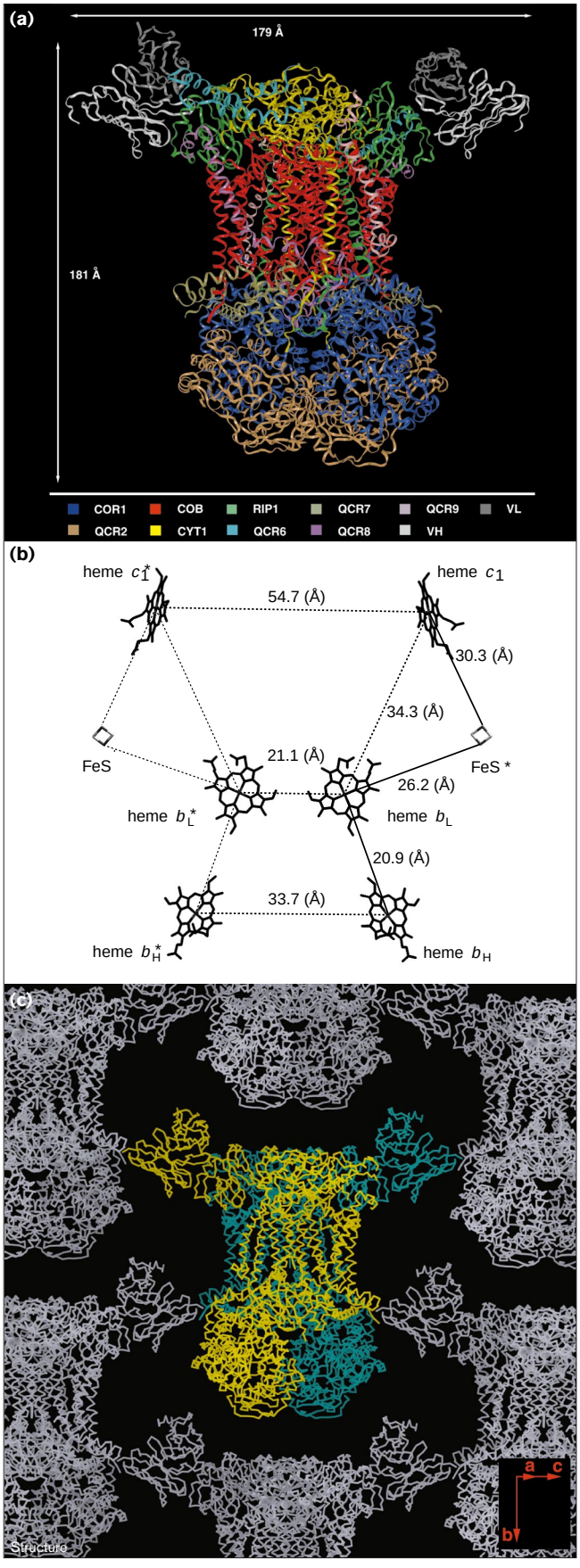

Figure 2

Structural model of the dimeric co-complex of the yeast cytochrome bc_1 complex and the bound $_{18E11}$Fv fragment. The molecule is viewed parallel to the membrane with the matrix side oriented to the bottom. The polypeptides are depicted as ribbon drawings. **(a)** Each monomer consists of nine subunits of the cytochrome bc_1 complex and two subunits of the Fv fragment, which are colour-coded. The figure was prepared using the program VMD [51]. **(b)** Relative locations of the redox centers in the dimeric cytochrome bc_1 complex viewed in the same orientation as (a). Cofactors are drawn as stick models and are marked with an asterisk for the second monomer. Distances between the iron positions are indicated with dotted or solid lines, the latter referring to distances important for electron transfer. **(c)** The crystal contacts of the co-complex in the (0.5a + c),b plane of the crystal lattice are mediated by the Fv fragment. The two monomers of the central cytochrome bc_1 complex are coloured in green and yellow, respectively. Neighbouring dimers are shown in grey.

For the comparison described above we used the coordinates (PDB code IBE3 [8]) of the bovine cytochrome bc_1 complex. This model includes all subunits and was refined at a resolution of 3 Å to an R factor of 26%. To evaluate the meaning of the rmsd we performed an alignment of the bovine and chicken complexes (PDB codes 1BE3 [8] and 1BCC [7], respectively): core 1 (1.2 Å rmsd), core 2 (1.1 Å rmsd), cyt *b* (0.8 Å rmsd), cyt c_1 (1.2 Å rmsd), su6 (1.2 Å rmsd), su7 (1.8 Å rmsd, su8 (1.1 Å rmsd), su9 (0.9 Å rmsd). Both the extrinsic domain as well as transmembrane region of the Rieske protein showed low rmsds (0.8 and 0.9 Å, respectively). The structure of the chicken cytochrome bc_1 complex (PDB code 1BCC) was determined at 3.2 Å with an R factor of 27%. The only known chicken sequence that could be used was that of cytochrome *b*. Although it has to be kept in mind that the chicken and bovine structures are at lower resolution and less well refined, the structural alignments of the C_α chains indicate a higher structural similarity when compared with yeast. Details of the yeast cytochrome bc_1 complex structure will be described below. Residue numbers given refer to the unprocessed subunits from the yeast complex to allow easy comparison with sequence numbers used in mutagenesis studies.

Transmembrane subunits, Rieske protein and QCR7

The transmembrane helices (A–H) of the highly conserved cytochrome *b* form the catalytical core of the cytochrome bc_1 complex. The redox centres heme b_L and heme b_H are bound between helices A, D, B and C. His82 and His183 are ligands of the heme b_L iron whereas His96 and His197 bind to the heme b_H iron. The assignment of these ligands as well as those of the other redox centres coincides with the results from sequence homology and functional studies [4]. In addition, the two different quinone/quinol-binding sites are located in this subunit (see below). Both sites are accessible from two large hydrophobic clefts at the dimer interface, which are formed by transmembrane helices of cytochrome *b*,

Table 4

Comparison between homologous subunits of the cytochrome bc_1-complexes from *S. cerevisiae* and *Bos taurus*

Yeast subunits*	MW (kDa)*†	No. of residues mature/precursor‡	Bovine homologue subunits‡	MW (kDa)	Number of TM§ yeast/bovine	Sequence alignment identity (similarity) (%)#	Structural alignment¶ yeast/bovine Rmsd¥(Å)/LALI**
COR1	47.4	431/26	Core 1	49	0/0	32.1 (51.0)	2.0 /417
QCR2	38.7	352/16	Core 2	45	0/0	27.6 (49.6)	2.6/336
CYT1	27.8	249 /61	cyt c_1	27.2	1/1	58.1 (77.6)	1.5/230
COB	43.6	385/–	cyt *b*	42.5	8/8	51.2 (75.7)	1.0/376
RIP1	20.1	185/30	ISP	21.5	1/1	51.2 (72.8)	1.0/122†† 3.0/47‡‡
QCR6	14.5	122/25	SU 8	11	0/0	39.7 (53.8)	1.5/106
QCR7	14.4	126/1	SU 6	14	0/0	35.9 (53.2)	2.5/77
QCR8	10.8	93/1	SU 7	9.5	1/1	22.1 (53.2)	1.8/62
QCR9	7.3	52/1	SU 10	7.2	1/1	38.2 (52.7)	2.4/51
QCR10	8.8	78/1	SU 11	6.4	nd/1	23.6 (45.5)	–
–			SU 9	8	–/0	–	–

*Subunit nomenclature and data are taken from the Yeast Protein Database [49]. †MW of the mature protein. ‡Homologous subunits are identified by structural comparison and are in accordance with a previous summary of corresponding subunits [4] and a report on subunit QCR10 [5]. §The number of transmembrane helices (TM) is taken from the known bovine [6,8] and the yeast structure presented here of the cytochrome bc_1 complex. #The amino acid sequence alignment was performed with the program *gcg* (version 8.1, Genetics Computer Group, Inc.): bestfit, gap weight 3.0, length weight 0.1, including signal sequences. ¶Structural alignment was done by superimposition of homologue subunits from the yeast structure and the 1BE3 coordinates [8] of the bovine protein using the DALI server [50]. ¥Rmsd is the positional rmsd of superimposed C_α atoms. **LALI is the total number of equivalenced residues. The Rieske protein was separately aligned for the extrinsic domain ††(residues 92–215 and 72–196 for yeast and 1BE3, respectively) and the transmembrane anchor ‡‡(residues 31–81 and 1–61 for yeast and 1BE3, respectively).

cytochrome c_1 and Rieske protein (Figure 3). Substrate exchange between bound and free quinone/quinol most probably takes place via these clefts.

The compact extrinsic domain of the Rieske protein (residues 93–215) is formed by three layers of antiparallel β sheets, which can be divided in a basefold (β strands 1–4 and 9–10) and a metal cluster binding fold (β strands 5–8). The [2Fe–2S] cluster is coordinated by Cys159, His161, Cys178 and His181 with Cys164 and Cys180 forming a disulfide bridge, which stabilizes the cluster [9]. The extrinsic domain is found in the *b* position, that is the cluster-bearing tip is in contact with cytochrome *b* of the second monomer and the [2Fe–2S] cluster is close to heme b_L. This orientation is caused by the binding of the inhibitor stigmatellin, which fixes the mobile domain ([7], see below). The domain is connected by a 'linker' region (residues 81–92) with its transmembrane anchor (residues 51–80). The structure of the N-terminal polypeptide of yeast and bovine/chicken complexes are different. The first ten residues form one strand of a β sheet to which cytochrome c_1, QCR8 and COR1 contribute. This secondary element is also present in the bovine subunit. The connecting loop (residues 40–50) to the transmembrane helix is nine residues shorter. The difference in the N terminus coincides with a low sequence homology. The sequence of the signal peptide is also very different. In yeast the nuclear encoded pre-protein is processed in two steps by a soluble matrix-processing peptidase and an intermediate peptidase [17], whereas the bovine precursor protein is processed in one step and the signal peptide is retained in the complex [8]. The location of the transmembrane helix is very similar in the complexes despite the low sequence homology.

Interestingly, the linker region forms a turn between Ala86 and Val88 that is best described as 3_{10} helix. Whereas the N-terminal residues including the helix-turn are stabilized by hydrogen-bond interactions, the C-terminal part of the linker forms an extended solvent-exposed chain. For the bovine complex a 3_{10} helix was described for the linker region, when the extrinsic domain is in the c_1 position (PDB code 1BE3 [8]). The stigmatellin-containing yeast structure probably represents the most extended conformation of the linker. These findings suggest that the single helix turn might direct helix formation of the elongated linker region when the extrinsic domain moves to the c_1 position.

The structure of the extrinsic domain is highly similar to the homologous domain of the bovine complex, as shown by the low rmsd of 1.0 and 0.7 Å for the structures 1BE3 (Table 4 [8]) and 1RIE [9], respectively. The higher similarity with the latter, is probably because of the better refinement of this structure at high resolution. Furthermore, in yeast the conserved Pro195, homologous to the bovine Pro175, is present in trans-conformation. A network of conserved salt bridges and hydrogen bonds is present in the connecting region between the base fold and cluster binding fold (e.g., Ser188–Asp143, Asp143–Arg121, Glu125–Arg119 and Gln141–Arg146). Thus, the conformation of the extrinsic domain from yeast in the *b* position resembles the closed

conformation found for the bovine domain in the c_1 position [8] or in the soluble form [9]. This suggests either that the extrinsic domain from yeast does not undergo internal conformational changes that are related to its movement, as proposed for the bovine complex [8], or that the open conformation described for the intermediate position in that three-state model is transient.

The contact between the cluster-binding tip of the Rieske protein and the complementary docking site of cytochrome *b* of the second monomer (cytochrome *b**) is stabilized by van der Waals forces and only a few hydrogen bonds in addition to the interactions with the ligand described below. Interestingly, a hydrogen bond is present between the conserved NZ-Lys288 of cytochrome *b** and the backbone oxygen of the second [2Fe–2S] cluster ligand His161. The Nε atom of this residue forms a hydrogen bond to a water molecule (W16), which itself is hydrogen bonded with the backbone oxygen of Lys288. Hydrogen bonds are present between the water molecules W16, W264* and O-Ile285 of cytochrome *b**. Additionally, ND2-Asn149 of cytochrome *b** is in hydrogen-bonding distance to O-Leu162 of the Rieske protein. Because the hydrogen bonds are close to the proposed substrate-binding site, the processes discussed below are likely to affect these bonds. This might aid release of the extrinsic domain from the *b* position.

Subunit QCR7 consists mainly of α-helical structural elements. It is docked on the surface of cytochrome *b* on the matrix side. The N terminus of the subunit is nine residues longer than of the homologous bovine subunit. It forms an additional α helix that encloses the C-terminal α helix of cytochrome *b*, which itself is five residues longer than in the bovine complex. Subunit QCR8 (one transmembrane helix) is associated with a number of subunits of the complex. The N-terminal part contributes one strand to the β sheet at the matrix side described above. It is ten residues longer than in the bovine subunit. The termini of both monomers are located antiparallel at the dimer interface on top of a V-shaped opening of the D helices of cytochrome *b*. Furthermore, the N terminus of QCR8 is in close contact with that of cytochrome *b* of the second monomer. The C terminus is in contact with the N terminus of cytochrome c_1 and with QCR6. The multiple interactions might be the reason that this subunit is important for the assembly of the complex [18].

Cytochrome c_1 and QCR6

In cytochrome c_1 the heme group is covalently attached to the polypeptide by thioether bonds with Cys101 and Cys104. His105 and Met225 form the fifth and sixth axial iron ligand. The subunit consists of seven α helices and two double-stranded β sheets. Given that the fold is similar to that of other members of the mitochondrial cytochrome *c* family [7], a nomenclature related to the

Figure 3

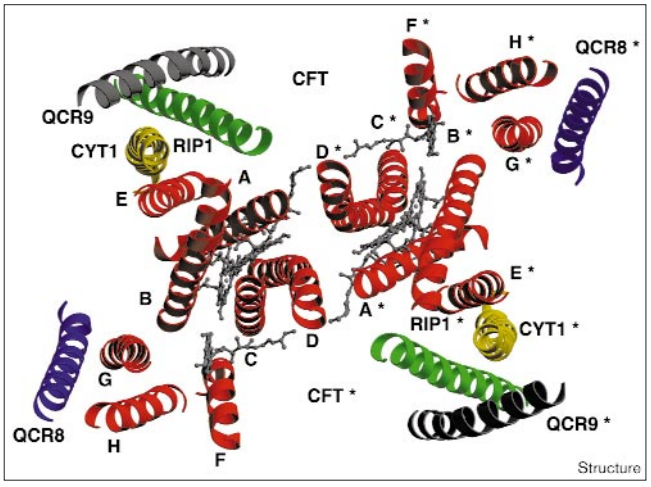

Helix packing in the transmembrane region of the cytochrome bc_1 complex viewed from the intermembrane side. The core of the complex is made up by eight helices of cytochrome *b* (red) which are labelled A–H. Rieske protein, cytochrome c_1, QCR8 and QCR9 are attached at the periphery and are marked with the subunit code. Asterisks are used for the second monomer. Two large hydrophobic clefts are present at the dimer interface (CFT). Heme b_L and heme b_H are bound between helix A, B, C and D of cytochrome *b*. The headgroup of the Q_o site inhibitor stigmatellin (between label B and C) is located close to heme b_L, the headgroup of coenzyme Q6 (behind helix A), close to heme b_H (shown as ball-and-stick models).

secondary structural elements of cytochrome *c* is used [9]: α1 (residues 87–102), α1′ (121–130), α1″ (162–171), α2 (179–184), α3 (188–196), α5 (244–261) and the transmembrane helix α5 (264–297). A distorted double-stranded β sheet (β1, β2) is present between the helices α4 and α5 and is characteristic for cytochrome c_1 [7]. The C-terminal residues Lys299 to Phe302 form a common β sheet with strands of subunit QCR1 and the N terminus of the Rieske protein, thus the transmembrane part and the matrix exposed subunit are firmly associated. A twisted loop between helices α1′ and α1″ forms an additional distorted double-stranded β sheet (Glu131 and Lys146), which is located close to the extrinsic domain of the Rieske protein (Figure 4). Acidic residues of this region were proposed to be involved in binding of cytochrome *c* on the basis of chemical labelling [19]. A similar conformation was described for the complex from chicken heart [7] whereas for the bovine protein [8] the existence of an extended α helix (α1′) and thus a shortened loop was published (Figure 4). As the amino acid sequence of cytochrome c_1 from chicken is not known but is expected to be similar to that of the bovine protein [7], it is not clear whether or not the loop can be present in different conformations. In the yeast complex, the mean temperature factor of this loop is higher than that of the complete subunit (89.3/57.9). The positions of mainchain and sidechain

atoms are well defined in the electron density map and we assume that this conformation is stable. Given that the conformation of the loop is the same in the structures of the chicken complex with the extrinsic domain of the Rieske protein located in different positions, it is most likely not influenced by this conformational change [7]. Furthermore, in yeast this loop mediates contact to the α1″ helix of cytochrome c_1 of the second monomer.

Subunit QCR6 has sequence similarity to the 'hinge' protein, a subunit of the bovine cytochrome bc_1 complex [20]. Whereas the latter is required for complex formation between isolated cytochrome c_1 and c [21], the yeast subunit is not essential for enzymatic activity. Deletion mutants are respiratory-competent but show only half of the normal enzymatic activity [22]. The subunit might enhance binding of cytochrome c. The general fold of QCR6 is similar to that of the bovine and chicken complexes, namely two antiparallel α helices (α1 Gln77–Gln110; α2 Cys123–Thr136). Their connecting loop is stabilized by a disulfide bridge, Cys101–Cys123, which is found in the same position as the hinge protein from bovine or chicken complexes. Thus, the loop is eight residues shorter in yeast, and in contrast to the latter complexes, the subunit does not possess a second disulfide bridge. Binding of cytochrome c is probably mediated by the N-terminal peptide, which is highly enriched in glutamic and aspartic acid residues as shown for the bovine cytochrome bc_1 complex [21]. No unequivocal electron density was observed for the first 48 residues of subunit QCR6. Similarly, the N terminus of the bovine hinge protein, which is 22 residues shorter, has not been included in the available models. The N-terminal peptide is probably mobile. This mobility might play a role in the docking of cytochrome c to the complex. The structures of the yeast and bovine cytochrome bc_1 complexes differ in the putative cytochrome c binding regions of cytochrome c_1 and QCR6. This finding is compatible with a sequence identity of yeast and bovine cytochrome c of 63%.

Core proteins

The two large so-called core proteins, COR1 and QCR2, are extramembranous subunits that are attached to the transmembrane domains and protrude into the matrix. Both subunits are bowl-shaped and assembled to a hollow ball with a crack-like opening on one side. They have a similar folding composed of an N- and a C-terminal domain (Figures 5a,b). Each of these domains consists of a mixed β sheet, that is surrounded by a number of α helices. The two domains are related by an approximate twofold axis. Sequence comparisons indicate that core proteins belong to the pitrilysin family, a group of Zn^{2+}-dependent metalloendopeptidases [23]. They are closely related by sequence homology to the matrix processing peptidases (MPP), which are also members of this family. MPPs are soluble heterodimeric proteins that are located in the mitochondrial matrix and cleave precursor proteins after their import into mitochondria [24]. The MPP β subunits contain the conserved inverse Zn-binding domain HXXEH (in single-letter amino acid code and where X denotes any amino acid) and the active site of the protease, whereas the α subunit is thought to bind and present the leader peptide. MPP activity requires both subunits. In plants the core proteins of the cytochrome bc_1 complex have a high MPP activity [25]. The sequence similarity indicates that the MPP α subunit is homologous to the core 2 protein and the β subunit to the core 1 protein. The core 1 protein of the fungus *Neurospora crassa* is identical to the MPP β subunit [26]. The bovine heart cytochrome bc_1 complex has a low MPP activity after additional detergent treatment of the complex [27]. In *S. cerevisiae* the two core proteins are proteolytically inactive but show sequence similarities to MPPs [28,29].

Although sequence homology is low between the corresponding subunits from bovine heart and yeast (Table 4) a superimposition of the structures demonstrates that their general folds are similar and that most secondary structural elements are present (Figures 5a,b). The differences

Figure 4

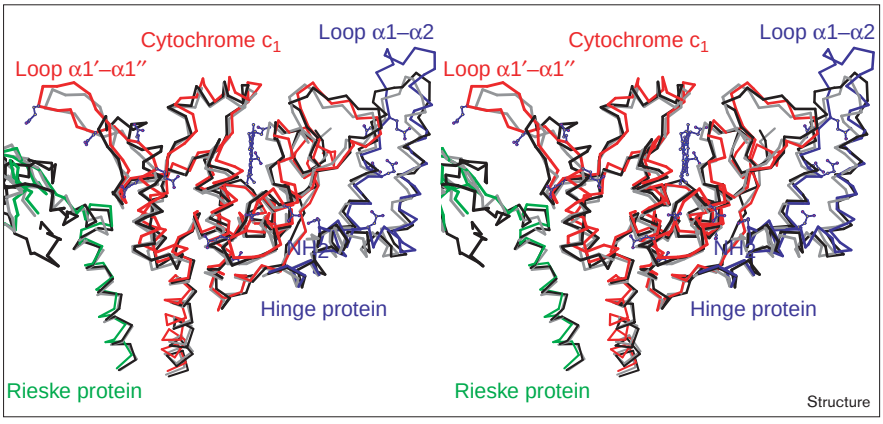

Putative docking region of cytochrome c (stereoview). Cytochrome c_1 (red), Rieske protein (green) and subunit QCR6 or hinge protein (blue) of the yeast cytochrome bc_1 complex were superimposed with the homologous subunits of the complexes from chicken (PDB code: 3BCC [7], grey) and beef (PDB code: 1BE3 [9], black). A part of the intermembrane region is shown with the intermembrane side on top. The backbone of the polypeptide chains is depicted as a stick model, heme c_1 as ball-and-stick presentation. Sidechains are shown for conserved acidic residues, which are presumably involved in binding of the substrate cytochrome c.

between the two species are most pronounced in the C-terminal domain of QCR2. The subunit is 68 residues shorter than the homologous bovine subunit. Its N-terminal domain has a five-stranded β sheet whereas the bovine core 2 protein has a six-stranded β sheet. The β sheet of the C-terminal domain is tilted in relation to the orientation of the bovine fold by approximately 15°. In the bovine complex the cleaved signal peptide of the Rieske protein (subunit 9) is located in the cavity between the core 1 and core 2 proteins [8]. The binding is stabilized by hydrophobic interactions with this β sheet [8]. Polar or charged residues are present at the corresponding positions in yeast. Furthermore, subunit QCR2 possesses a short, slightly disordered loop (instead of an αL helix and an extended loop), which protrudes into the cavity between the bovine core 1 and core 2 subunits (Figure 5b) and contributes to binding of subunit 9. Thus, this cavity is larger in yeast and open to the bulk solvent and no electron density was found for a retained signal peptide. Further differences exist in the C-terminal region. COR1 and the bovine core protein 1 are more similar to each other than are QCR2 and the bovine core protein 2. The putative Zn-binding site of the bovine core protein 1 consists of two α helices [8] that are also present in yeast. Asn70, Asn74 and Gln137, however, are located at the position of the Zn-binding triad instead of Tyr57, His61 and Glu137. In addition, the yeast subunit lacks the loop Phe64–Asn73 of the bovine homologue. This loop is located close to the metal-binding site and in direct neighbourhood to the above described region of the αI helix of core protein 2, which is important for binding of subunit 9. Core proteins are thought to be relics of a protease, which was originally integrated into the cytochrome bc_1 complex and later lost its proteolytic activity when soluble forms of processing peptidases evolved after a detachment event [30]. Loss of processing activity might have occurred first in yeast. It is noteworthy that the sequence identity of the bovine core proteins to the related MPP subunits of yeast is significantly higher than that of the yeast subunits itself (core protein 1 / β-MPP, 38%; COR1 / β-MPP, 27%; core protein 2 / α-MPP, 27%; QCR2 / α-MPP, 21%). Besides the catalytic residues further structural elements described above might have been of importance for recognition and binding of the substrate. For example, the sequence of the loop Phe64–Asn73 is identical in the bovine core protein 1 and the yeast β-MPP, thus supporting its possible functional importance. The two core proteins of the yeast cytochrome bc_1 complex are not involved in cytochrome *c* reductase or MPP activity. Mutants with structural defects in COR1 or QCR2 fail to properly assemble the complex [28,29,31]. This might explain why these subunits were retained during evolution.

Figure 5

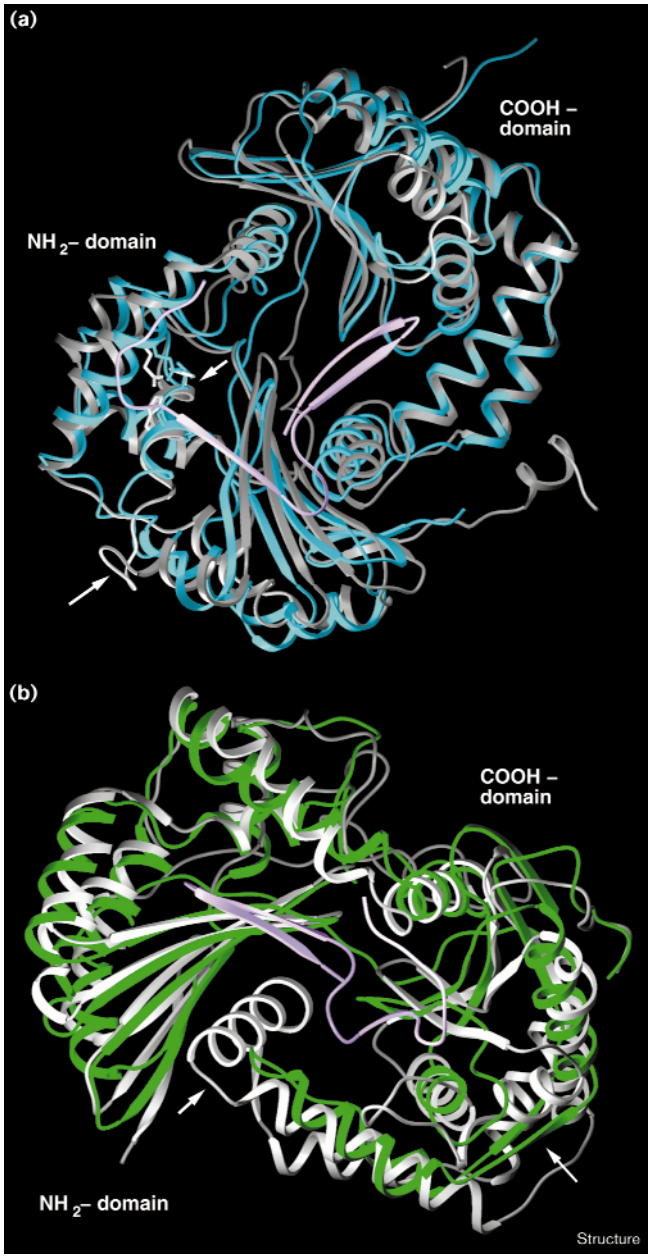

The folding of subunits COR1 and QCR2 of the yeast cytochrome bc_1 complex in comparison with the homologous subunits of the bovine complex (PDB entry 1BE3 [9]). **(a)** Subunit COR1 (cyan) is viewed in an orientation parallel to the membrane with the matrix side at the bottom. The QCR2 contact area points towards the front. Bovine subunit 9 (violet) and core 1 protein (grey) were superimposed. **(b)** Subunit QCR2 (green) and the superimposed bovine subunit 9 (violet) and core 2 protein (light grey) are viewed from the intermembrane side. Differences in the fold discussed are marked with an arrow.

Q_o site

The cytochrome bc_1 complex from yeast was crystallized in the presence of the Q_o-site-specific inhibitor stigmatellin. This molecule is thought to mimic the monoprotonated doubly or singly reduced quinone, an intermediate of the ubiquinone redox reaction as shown for the Q_B site of the

reaction center from *Rhodopseudomonas viridis* [32] and proposed as well for the cytochrome bc_1 complex [33,34]. F_o–F_c electron-density maps calculated prior to inclusion of the inhibitor molecule into the model allowed us to unambiguously identify the orientation of the molecule (Figure 6a) and the residues that are involved in the formation of the binding pocket. The binding site of stigmatellin is located at the intermembrane side of the protein close to the border of the hydrophobic core of the transmembrane region in proximity to heme b_L on one side and the [2Fe–2S] cluster on the other side (Figure 6b). The binding pocket is formed by the *ef* loop of cytochrome *b* and its cd_1 helix, which surround the chromone ring of the inhibitor molecule. In addition, the [2Fe–2S] cluster presenting tip of the extrinsic domain of the Rieske protein of the second monomer of the complex (Rieske protein*) contributes to pocket formation. The stigmatellin tail stretches into the large hydrophobic cleft formed by the two halves of the dimer and is stabilized by hydrophobic interactions with nonpolar residues. The chromone ring and tail are surrounded by nonpolar residues (Ile269, Val146, Met295, Phe296, Ala126, Phe129, Pro271, Phe278, Ile125, Ile147 and Leu165) of cytochrome *b* (Figure 6c). An average B factor of 37.0 Å^2 for the inhibitor molecule compared with 35.2 Å^2 for the neighbouring residues indicates the tight interaction of the molecule with residues of the binding pocket. Mutations of nonpolar residues within the binding pocket affect inhibitor binding as well as quinol oxidation: for example, the mutations Ala126→Thr, Ile147→Phe, Leu275→Phe and Phe129→Leu, result in Q_o-site inhibitor resistance whereas Phe129→Leu also leads to slow quinol oxidation [13]. These results support the view that the binding pockets for stigmatellin and ubiquinol are the same.

Hydrogen-bond interactions are found exclusively for the carbonyl group O4 and the hydroxyl group, which is labelled O8 in our model. The carbonyl oxygen (O4) is hydrogen-bonded to Nε-His181 of the Rieske protein*. This residue is a ligand of one iron atom of the [2Fe–2S] cluster via the Nδ atom. A donor–acceptor distance (D–A) of 2.7 Å was determined for the Nε-O4 interaction. Because this bond is within the plane of the histidine ring and along the bisector of the CE1–NE2–CD2 angle, it is obvious that the Nε atom has to be protonated and acts as the donor. His181 of the Rieske protein is essential for integrity and enzymatic activity of the complex. The hydroxyl group (O8) is hydrogen bonded to OE1 of Glu272 (D–A 2.7 Å), O8 serves as donor and OE1 as acceptor. Glu272 is completely conserved in mitochondrial cytochrome *b* [35]. Mutation of the homologous glutamate residue in *Rhodobacter sphaeroides*, namely Glu295→Asp, Glu295→Gly and Glu295→Gln, did not only result in stigmatellin resistance but also led to a slower or even completely abolished ubiquinol oxidation [13]. This finding supports the assumption [32] that the binding of stigmatellin resembles the binding of an intermediate form of the ubiquinol oxidation with the quinone characteristic carbonyl group liganded to His181 of the Rieske protein* and the ubiquinol characteristic hydroxyl group liganded to Glu272 of cytochrome *b*. The interaction with these two residues might help to stabilize the enzyme–substrate complex.

During oxidation of ubiquinol one electron will be transferred to the [2Fe–2S] cluster and the second electron to heme b_L while two protons are released. The distance between the iron atom of the heme b_L and the hydroxyl-group of stigmatellin (O8) is 14.8 Å. This distance will allow a reasonably fast direct electron transfer from a comparably oriented ubiquinol molecule. Water molecules (W107 and W45) and the hydroxyl group of Tyr132 of cytochrome *b*, however, are as close as 2 Å to the connecting axis. Thus, the question arises, are amino acid residues and water molecules between the heme group and the prospective ubiquinol-binding site involved in electron- and/or proton transfer? Pathways for proton release have to exist because the binding site is located within the nonpolar core of the transmembrane region.

The binding pocket of *heme* b_L is built by nonpolar residues (Leu40, Phe89, Gln43, Pro187, Thr127, Tyr184, Ala 51, Gly47, Ala86, Ala83, Gly131, Tyr132 and Val135) with the exception of the iron ligands (His82 and His183). The heme propionate groups point towards the intermembrane space and are part of a network of hydrogen bonds connected to the bulk solvent (Figure 6d). The carboxyl group of propionate A appears to be involved in four hydrogen bonds with reasonable geometry and distance. The oxygen O1A accepts one hydrogen bond from the NH1 atom of the neighbouring Arg79 and probably from the O1A of the carboxyl group of propionate D. This propionate is surrounded by nonpolar residues and is presumably protonated. Stabilizing electrostatical interactions of the guanidino group between Arg79 and the propionate carboxyl are possible. The oxygen O2A of propionate A accepts two hydrogen bonds of the water molecules W73 and W42. The position of W73 is stabilized by hydrogen-bond interaction with the amino group of Asn256. This water molecule is connected via hydrogen bonds to a network of water molecules within a cleft that opens into a cavity at the interface of cytochrome *b* and cytochrome c_1. This cavity is formed by a part of the *ef* loop (residues 246–257) and short stretches of helices C and cd_1 (residues 131–143) of cytochrome *b* and the residues 259–270 of cytochrome c_1. The cavity is filled with water molecules. These water molecules form hydrogen bonds among themselves and with polar and charged sidechains as well as with mainchain atoms. The cavity is open to the bulk solvent at two sides. If the *heme* b_L propionates change their protonation state during the redox cycle a proton uptake would be most likely to occur via the O1A atom of propionate A.

Figure 6

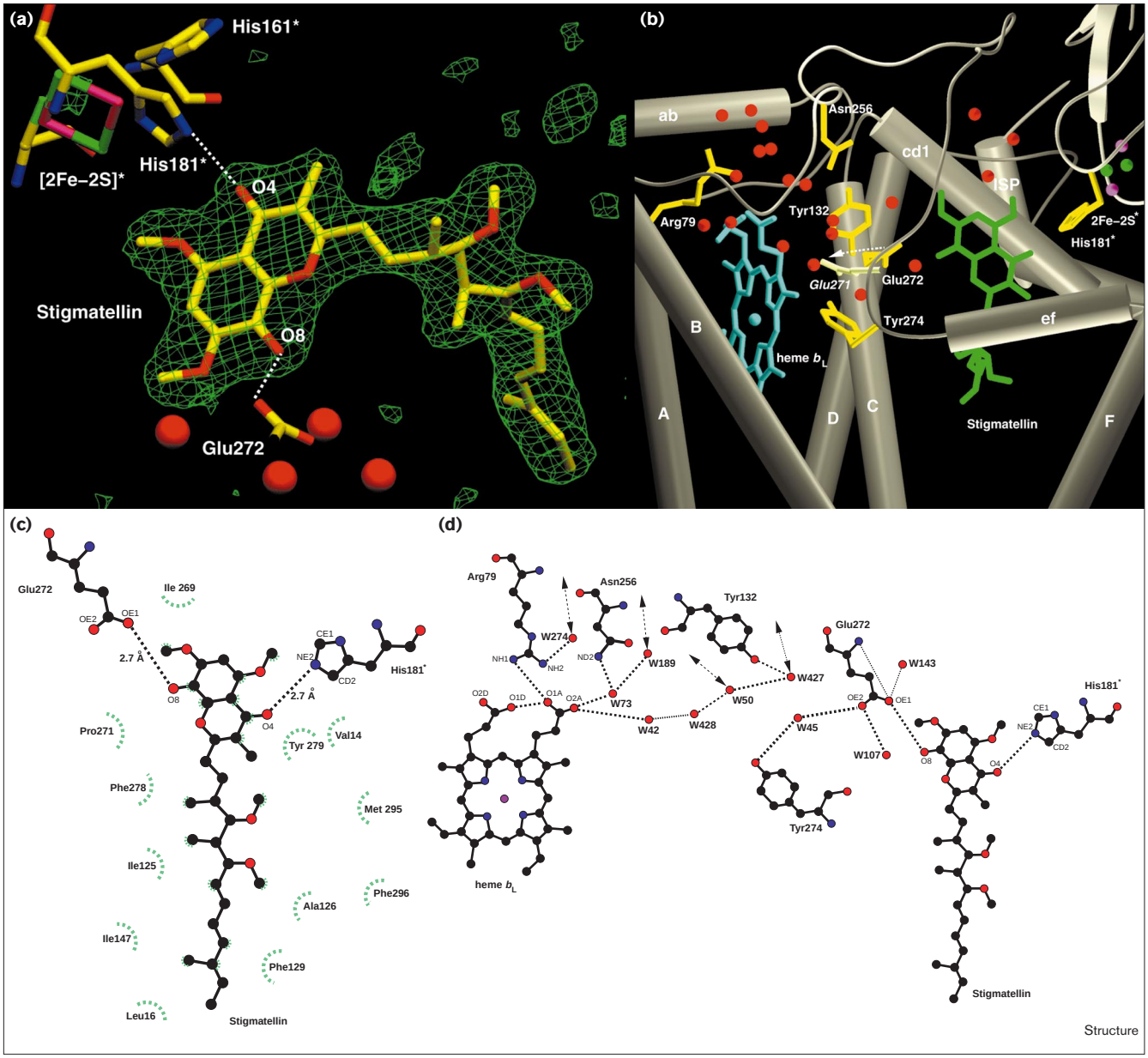

The Q_o site of the cytochrome bc_1 complex with the bound inhibitor stigmatellin. **(a)** The difference density map (green) was calculated with coefficients F_o–F_c after omitting stigmatellin and is contoured at 3σ. The carbonyl oxygen and the hydroxyl group of stigmatellin are labelled O4 and O8, respectively. The [2Fe–2S] cluster and its coordinating amino acid residues of the second monomer are shown on top, Glu272 of cytochrome *b* is shown below. **(b)** Q_o site with parts of cytochrome *b* (grey) and the Rieske protein of the second monomer (light grey). Helices are shown as tubes and labelled as described before, β strands as ribbons, loops as ropes, and water molecules as balls (red). Sidechains of residues involved in hydrogen-bond interactions are shown. The intermembrane side is at the top of the figure and the model is viewed parallel to the membrane. Helix *ab, cd1* and *ef* of cytochrome *b* are parallel and slightly tilted to the membrane plane. The sidechain of residue Glu271 (homologous to yeast Glu272) is taken from the superimposed model of the bovine protein (PDB entry 1BE3 [9]), which does not contain stigmatellin. **(c)** Schematic presentation of the binding pocket. Hydrogen bonds are present exclusively between the carbonyl oxygen of stigmatellin and His181* of the Rieske protein* as well as the hydroxyl oxygen and OE1 of Glu272 (cytochrome *b*). Hydrophobic interactions with neighbouring residues are indicated (green dashed lines). Interactions were determined using the programs *hbp* and *ligplot* [51]. Atoms are colour-coded as follows: black, carbon; blue, nitrogen; red, oxygen. All residues but His181* (Rieske protein) belong to cytochrome *b*. **(d)** Apparent hydrogen-bonding network at the Q_o site. Hydrogen bonds with appropriate geometry and distances [52] are indicated by dashed lines, bonds with less favourable geometry as dotted lines. Arrows are used for indicating hydrogen-bond interactions with a network of water molecules that have access to the bulk solvent.

Tyr132 and Tyr274 are positioned between *heme* b_L and the hydroxyl group (O8) of stigmatellin (Figure 6d). The water molecule W427 is in hydrogen-bond distance to OH-Tyr132. This water molecule interacts on one side with water molecules located in the cleft and the cavity described above. Secondly, it appears to be hydrogen bonded to the water molecule W50. This water molecule is close to the interface of cytochrome *b* and cytochrome c_1 and has access to the bulk solvent via further water molecules. In contrast, OH-Tyr274 probably donates a hydrogen bond to W45 and is not directly connected to other water molecules. Apparently, W45 donates a hydrogen bond to OE2-Glu272 , which accepts another bond from W107. The OE1 atom of Glu272 that binds stigmatellin might accept a hydrogen bond either from the mainchain nitrogen of the residue or from water molecule W143. However, the bond angles of both are are not very favourable for hydrogen bonding. Additional hydrogen bonds with mainchain atoms stabilise the water molecules that interact with Glu272. These water molecules are not connected to the bulk solvent or to a network of water molecules. If Glu272 acts as proton acceptor during ubiquinol oxidation, the proton would get stuck there without further changes. Two scenarios are probable. Firstly, after electron transfer from ubiquinol to the [2Fe–2S] cluster, His181 (His161 in beef) is present in the protonated form [33,34] as supported by the binding of stigmatellin. The extrinsic domain of the Rieske protein is thought to change its position and to move close to cytochrome c_1 [6–8] where the proton is expelled after reoxidation of the redox center [34]. After full oxidation ubiquinone might leave the binding site and Glu272 might become accessible to the bulk solvent. Secondly, a movement of residues involved might change the hydrogen bonded network pattern and allow the proton to be released. There is evidence for the latter assumption as the sidechain of Glu271 (the residue homologous to Glu272 in yeast) is found in the stigmatellin-free structure of the bovine cytochrome bc_1 complex in a different position, whereas the location of most of the surrounding residues including Tyr131 and Tyr273 is the same as that of the homologous residues in yeast (Tyr132 and Tyr274). If the Glu271 orientation is superimposed onto the yeast structure (Figure 6b), its carboxyl group points towards the heme propionate A into the region that contains water molecules stabilized by hydrogen bond interactions with Tyr132 and Tyr274 (Asn256). These residues and water molecules are connected with the bulk water at the interface of cytochrome *b* and cytochrome c_1 via the two described hydrogen-bonded networks of water molecules. Thus, if Glu272 acts as a primary proton acceptor it might then donate the proton to a network of hydrogen bonded water molecules thereby expelling into the intermembrane space. It could be localised close to the heme propionates when heme b_L is reduced and can be stabilized by the negative charge of the electron at the heme. When the electron is transferred from heme b_L to heme b_H it should be released to the bulk phase.

Although Glu272 is completely conserved in mitochondrial cytochrome *b* [35], it is not essential for the electron transfer between quinol and heme b_L. Mutations of the homologous residue Glu295 in *R. sphaeroides* for example Glu295→Asp, Glu295→Gly, resulted in stigmatellin resistance and slow quinol oxidation, but did not completely block ubiquinol oxidation. The latter is the case for the mutation Glu295→Gln [13]. The residues Tyr132, Tyr274 and Arg79 are highly conserved in mitochondrial

Figure 7

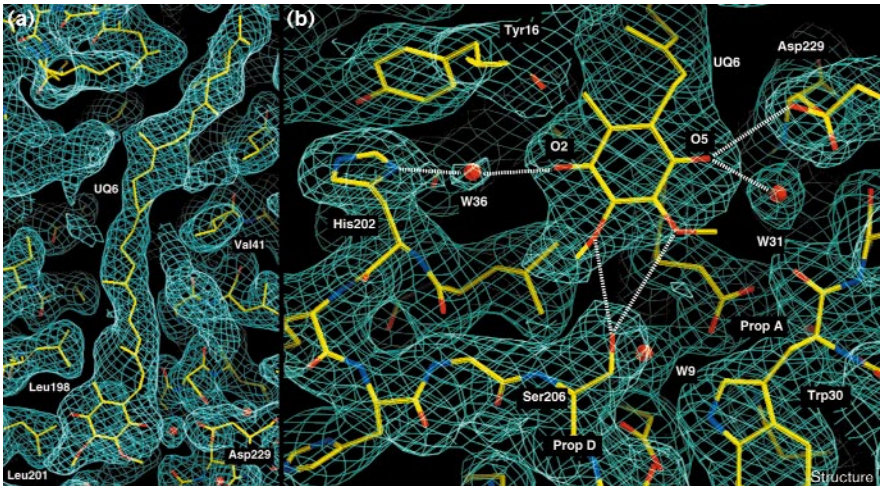

The Q_i site binding site containing the natural substrate coenzyme Q6 (UQ6). **(a)** Refined model and $2F_o–F_c$ electron-density map after inclusion of UQ6 viewed parallel to the membrane with the matrix side at the bottom. The isoprenoid tail of UQ6 protrudes along helix A and D of cytochrome *b* into the lipophilic cleft between the two monomers. **(b)** Binding pocket of the ubiquinone headgroup. UQ6 is oriented nearly in a right angle to the porphyrin plane of heme b_H. The bent propionate A of the heme (Prop A) forms part of the binding pocket and stabilizes the quinone ring plane by hydrophobic interaction. Polar interactions of the UQ6 carbonyl oxygens are present on one side to Asp229 (O5–OD2 3.6 Å) and a water molecule (O5–W31 3.3 Å) and on the other side via a water molecule (W36) to His202 (O2–W36 3.3 Å, W36–H202 2.6 Å) of cytochrome *b*. The map is contoured at 1.0σ; atoms are shown in standard colours.

cytochrome *b* [35]. Although they are not likely to be involved directly in binding of ubiquinol, mutations in these residues led to disturbance of quinol oxidation, which might be explained by an impaired proton release. Mutations of Tyr297, the bacterial homologue to Tyr274 and to Tyr147 (homologous to Tyr132), for example Tyr297→Ser, Tyr297→Phe, Tyr147→Phe and Tyr147→Val, resulted in slow quinol oxidation. The change of Tyr147 to alanine or serine completely abolished quinol oxidation [13]. These results demonstrate the importance of these residues. Thus, we assume that the putative ubiquinol ligands His181 and Glu272 probably act as primary proton acceptors during ubiquinol oxidation. Release of protons occurs after movement of the Rieske domain and the glutamate residue as was proposed previously [34]. The other residues that are discussed might have a role in proton transfer either directly or via stabilization of the hydrogen bond chain. Shifting the proton in the same directions as the electrons might be of advantage for electrostatic reasons and speed up proton transfer.

Q_i site

A pronounced elongated feature was present in the F_o–F_c electron-density map close to heme b_H. Coenzyme Q6 (UQ6) is the natural substrate of the yeast cytochrome bc_1 complex and fits completely into the electron density. The position is in accordance with the reported binding of Q_i site specific inhibitors in bovine and chicken cytochrome bc_1 complexes [6–8]. A model of UQ6 was introduced and refined (Figure 7). The ubiquinone headgroup is embedded into a binding pocket at the matrix side of the transmembrane region formed by parts of helix A, D, E and *a* of cytochrome *b* and heme b_H. The binding pocket is shielded from the matrix side by two distorted β strands formed by the *de* loop and an N-terminal peptide (Ser20 to Ile26) of the same subunit. It is open towards the membrane core, thus allowing the substrate and product molecules to enter or leave the site. The electron density for the isoprenoid tail of UQ6 in the F_o–F_c electron-density map prior to the insertion of the model as well as in the final $2F_o$–F_c electron-density map was uninterrupted. The tail protrudes into the cleft, which is formed by the two monomers. It stretches out along helix D with the residues Phe188, Ala191, Val194, Leu198 and Leu201 pointing towards the tail on one side and helix A with residues Leu40, Val41, Ile44, Val45, Ile48 and Phe49 on the other side. Thus, the end of the isoprenoid tail is close to the stigmatellin tail that is bound to the Q_o site of the second monomer. In addition, residual elongated electron density features are present in the hydrophobic cleft. They might result from alternative orientations of the isoprenoid tail.

The plane of the ubiquinone ring can be identified exactly. It is at nearly 90° to the porphyrin plane of heme b_H. The determination of the exact positions of the carbonyl and methoxy groups is more difficult, however, because the electron-density map does not show separate densities for the individual methoxy- and carbonyl-groups of the quinone. The model of UQ6 was introduced in several alternate orientations and refined. Figure 7b shows the best and most stable orientation. Remarkably, the carbonyl oxygens of the ubiquinone and the iron atom of heme b_H nearly form an isosceles triangle with a distance to the iron atom of 9.8 Å for each of the prospective carbonyl oxygens. The bound ubiquinone is stabilized perpendicular to the ring plane by hydrophobic interactions. On one side of the binding pocket Met221 points towards the substrate. This residue is substituted in most mitochondrial cytochrome *b* subunits by phenylalanine [35], which can serve the same function. On the opposite side the bent propionate A of heme b_H is located. Within the plane of the ubiquinone ring the spacious binding pocket is formed by polar residues with the following sidechains pointing towards the substrate: Ser20, Gln22, Asn31, Ser34, Ser206, Asp229 and His202. Few residues are close enough to stabilize the substrate–protein complex. The methoxy positions O3 and O4 are 3.4 Å and 4.1 Å away from the hydroxyl group of Ser206, respectively. In our model Asp229 is closest to the O5 carbonyl oxygen of UQ6 (OD2–O5 3.6 Å). Furthermore, a water molecule (W31) is in hydrogen-bonding distance to this carbonyl oxygen. A protonated Asp229 could help binding the ubiquinone by providing a hydrogen bond and might act as proton donor during reduction of the substrate. The second carbonyl oxygen O2 is in hydrogen-bonding distance to a water molecule (W36), that itself is hydrogen bonded by Nδ of His202. His202 stabilizes the binding of ubiquinone indirectly and might serve as direct or indirect second proton donor. Both residues belong to the most highly conserved residues in mitochondrial cytochrome *b* [35].

The donors have to be reprotonated from the matrix. This is unlikely to occur directly from the bulk solvent, as examination of the binding pocket for pores of a suffient size using a cavity map contoured at 2.5σ provided a negative result. Protons abstracted from His202 via the water molecule W36 could be replenished by reprotonation of the sidechain, as it points towards the surface at the dimer interface. A reprotonation of His202 in this conformation appears unlikely, however, because the Nε atom is directed towards the N terminus of the subunit QCR8*. One possibility is that a movement of the histidine sidechain allows its reprotonation and/or opens a connection between the binding pocket and the bulk solvent. This would allow water molecules to enter the pocket when the product leaves leading to the reprotonation of His202 and Asp229. Interestingly, in the ubiquinone-free structure of the bovine cytochrome bc_1 complex (PDB entry 1BE3 [8]) the sidechain of His201 (homologous to His202) is bent into the binding site, whereas the sidechain of Asp228 (homologue Asp229) is present in a similar orientation. In our model this orientation would

bring the imidazole nitrogen as close as 2.2 Å to the carbonyl oxygen O2. Thus, His202 could interact indirectly or directly and stabilize ubiquinone and/or its reduction intermediates, and might act as proton donor. A movement of the sidechain might be required. The different orientation in the bovine model might indicate that a movement of the histidine sidechain is possible. Alternatively, the different orientation might depend on the species. It should to be noted that, in yeast, the His202 sidechain is stabilized in its position by the aromatic sidechain of Tyr16, which is present in a parallel orientation. This residue is not conserved in mitochondrial cytochrome *b* [35] and the homologous bovine Ala17 has no stabilizing effect.

Taking into account the equidistance of the ubiquinone carbonyl oxygens to the heme b_H iron, and the existence of two proton donors it seems probable that after substrate binding electron- and proton-transfer can take place without rotating the ubiquinone ring out of the plane. It is possible that during the reduction the headgroup can be present in different orientations within the plane. This would allow the transient formation of stabilizing hydrogen bonds with substrate and reduction intermediates. The B factor of the refined coenzyme Q6 (80.7 Å^2) is high compared with the average B factor of cytochrome *b* (35.4 Å^2). This observation might be because of a partially occupied binding site. The protein preparations used for crystallization were partly depleted in phospholipids and thus in ubiquinone (unpublished observations). Furthermore, this effect might be caused by a higher mobility of the ligand if the stabilizing hydrogen-bond interactions are weak, or caused by alternative conformations of the ubiquinone and/or its reduction products. Further experiments have to show whether or not a reorientation of UQ6 and a movement of His202 are involved and allow protonation and/or water entrance.

Biological implications

The cytochrome bc_1 complex is an oligomeric membrane protein complex that is a component of respiratory and photosynthetic electron transfer chains. The enzyme couples electron transfer from ubiquinol to cytochrome *c* with the generation of a proton gradient across the membrane.

The mitochondrial cytochrome bc_1 complex from yeast is a homodimer. Each monomer consists of three catalytic and seven additional subunits and contains four redox centres. The catalytic mechanism of the enzyme [10,11] involves two catalytic sites. Quinol oxidation takes place at the Q_o site. In a split electron transfer pathway one electron is used for cytochrome *c* reduction (via a [2Fe–2S] cluster and cytochrome c_1) and the second electron is transferred to the Q_i site (via heme b_L and heme b_H). Here, quinone is reduced in two steps to quinol and protons are taken up from the matrix side. Quinol oxidation leads to proton release to the intermembrane side.

The cytochrome bc_1 complex from the yeast *Saccharomyces cerevisiae* was crystallized together with a bound antibody Fv fragment. This approach is useful to obtain well-ordered crystals of membrane proteins [14–16]. The structure of the cytochrome bc_1 complex and the bound Fv fragment was determined at a resolution of 2.3 Å. The model includes the Q_o site inhibitor stigmatellin, endogenous coenzyme Q6 at the Q_i site and 346 water molecules. A comparison with the structures of the bovine and chicken cytochrome bc_1 complexes showed that the catalytic subunits exhibit highest homology. Pronounced yeast-specific features were found for the putative cytochrome *c* docking site and a number of differences are present in the additional subunits. Superimposition of the two large subunits COR1 and QCR2 with the homologous bovine subunits suggests sites that might have been of importance for former endopeptidase activity.

The binding of stigmatellin is thought to resemble the binding of an intermediate of ubiquinol oxidation [32]. The carbonyl group and the hydroxyl group are hydrogen bonded to His181 of the Rieske protein of the second monomer and Glu272 of cytochrome *b*, respectively. His181 is a ligand of the [2Fe–2S] cluster. The interaction of these two residues might help to stabilize the enzyme–substrate complex and they might act as primary proton acceptors. A network of hydrogen bonds between polar residues and water molecules at the Q_o site might be involved in proton release. Coenzyme Q6 is bound in a spacious binding pocket at the Q_i site. The carbonyl oxygens are closest to Asp229 and a water molecule, which is hydrogen bonded to His202 of cytochrome *b*. The two residues most likely act directly or indirectly in stabilizing ubiquinone and/or its reaction intermediates and might act as primary proton donors. Possible pathways of proton uptake are discussed.

The high-resolution structure of the yeast cytochrome bc_1 complex allows a combined approach of X-ray crystallography, biochemistry, spectroscopy and mutagenesis to understand structure-function relationship of this important membrane protein. Given that inhibitors of the complex are used as fungicides, the structure might aid further development of suitable compounds.

Materials and methods

Protein purification, co-complex preparation and crystallization

The cytochrome bc_1 complex from yeast was prepared essentially as described for the cytochrome bc_1 complex from potato [36]. In short, membranes were solubilized with dodecyl-β-D-maltoside (DDM) and unsolubilized material was discarded after centrifugation (30 min, 150,000xg). The complex was purified with a DEAE-Sepharose (FF) column using a 380–500 mM NaCl gradient followed by size-exclusion chromatography (SepharoseCL-6B). The highly purified and active complex was used to raise monoclonal antibodies (unpublished observations). The corresponding Fv fragment of the monoclonal antibody $_{18E11}$mAB was cloned and expressed in *Escherichia*

coli using the plasmid pASK68 [37]. The fragment was purified by streptavidin affinity chromatography [37].

For crystallization purposes the cytochrome bc_1 complex containing fractions of the first anion exchange chromatography step were diluted 2.4-fold with salt-free buffer (50 mM potassium phosphate pH 6.9, 0.01% DDM) and then applied to a DEAE-HyperD (BIOSEPRA) column (7.5 mm × 7.5 cm) using an high-performance liquid chromatography (HPLC) system (Biosys 2000, Beckmann) with a flow rate of 2.0 ml/min. Cytochrome bc_1 complex inhibitors were added prior to diluting the enzyme. The bound protein was washed with 15 column volumes buffer (50 mM potassium phosphate pH 6.9, 0.05% undecyl-β-D-maltoside [UDM], 150 mM NaCl) and eluted using a two-step salt gradient from 150–300 mM and 300–500 mM NaCl. The cytochrome bc_1 complex containing fractions were pooled, mixed with the purified $_{18E11}$Fv fragment at a molar ratio of 1:1.4 and incubated on ice for 30 min. The surplus Fv fragment was separated by size-exclusion chromatography using a TSKgel G 4000 SW column (TosoHaas) and the co-complex containing fractions were pooled and concentrated. The protein solution was mixed with varying amounts of precipitant (PEG 4000, 100 mM Tris-HCl, pH 8.0, 0.05% UDM) and crystals were obtained using the vapour diffusion technique against 5–6% PEG 4000.

Data collection

Data were collected at the synchrotron beamlines indicated in Table 1. They were processed with DENZO of the HKL program suite [38,39]. The processed data were merged using SCALEPACK. Structure factors were calculated from the measured intensities employing the program TRUNCATE from the CCP4 package [40] and an overall temperature factor B_{Wilson} was determined.

Molecular replacement, isomorphous replacement and density modifications

Molecular replacement was performed as implemented in the X-PLOR program package [41]. Before the translational search a Patterson correlation (PC) refinement was used to filter the peaks of the rotational search [42]. To refine heavy-atom sites and calculate phases the program MLPHARE of the CCP4 package was used [40]. The mercury and silver derivatives have several of their heavy-atom sites in common, thus their contributions in improving the phases was limited. The iridium-derivative added completely different sites and despite its low phasing power was essential for the quality of the final experimental electron-density map. The phases were improved by solvent-flattening using the program DM [43] and in the process of mask-generation extra density showed up that was large enough to accommodate the Fv fragment. Prior to model building the automated refinement procedure ARP/wARP [44] was used to obtain a clearer electron-density map, involving a process of iterative improvement by placing and refining water molecules in the electron-density map.

Model building and refinement

Based on the experimental electron-density map chain tracing and polyalanine model building were performed using the XtalView software program [45] for major parts of the cytochrome bc_1 complex subunits and the two polypeptide chains of the $_{18E11}$Fv fragment with the exception of nearly half of subunit QCR2; the cofactors were included. The program O [46] was used to introduce identifiable amino acid residues. Refinement was carried out initially for data up to 2.5 Å resolution with the pre-release version 0.4 of CNS [47]. 2.5% of the measured data were used as test set to calculate the R_{free} [48]. Simulated annealing was performed using the standard slow cooling protocol (temperature bath coupling, molecular dynamics from T = 3000 to 0K with velocity scaling every 25 fs, and integration step of 0.5 fs). In the later stage of refinement temperature factors were refined after each annealing run. Refinement was interlaced with model building sessions using the program O. After iteratively improving model, model phases and electron-density maps the trace and sequence assignment for the model of all polypeptide chains of the co-complex were completed. After refinement of the model at 2.3 Å resolution 346 solvent molecules were added by identification of peaks > 3 σ in F_o–F_c difference electron-density maps using the CNS program when the geometry was suited for hydrogen bonding. Finally, refinement converged to an R_{free} of 25.4% and a conventional R value of 22.2%.

Accession numbers

The coordinates have been deposited in the Protein Data Bank (entry code 1EZV).

Acknowledgements

We thank W Grabarse for helpful discussions, CRD Lancaster and U Ermler for support during crystallographic work, and H Betz and D Vinzenz for technical assistance. We gratefully acknowledge support by the staff of the synchrotron facitlities at the ESRF, Grenoble, France, at the EMBL/DESY, Hamburg, Germany, and at the MPG-BW6/DESY, Hamburg, Germany. This work was supported by the BMBF and by the Fonds der Chemischen Industrie.

References

1. Hatefi, Y. (1985). The mitochondrial electron transport and oxidative phosphorylation system. *Ann. Rev. Biochem.* **54**, 1015-1069.
2. Brandt, U. & Trumpower, B.L. (1994). The proton motive Q-cycle in mitochondria and bacteria. *CRC Crit. Rev. Biochem.* **29**, 165-197.
3. Schägger, H., Link, T.A., Engel, W.D. & von Jagow, G. (1986). Isolation of the eleven protein subunits of the bc_1 complex from beef heart. *Methods Enzymol.* **126**, 224-237.
4. de Vries, S. & Marres, S.A.M. (1987). The mitochondrial respiratory chain of yeast. Structure and biosynthesis and the role in cellular metabolism. *Biochim. Biopys. Acta* **895**, 205-239.
5. Brandt, U., Uribe, S., Schägger, H. & Trumpower, B.L. (1994). Isolation and characterization of QCR10, the nuclear gene encoding the 8.5-kDa subunit 10 of the *Saccharomyces cerevisiae* cytochrome bc_1 complex. *J. Biol. Chem.* **269**, 12947-12957.
6. Xia, D., *et al.*, & Deisenhofer, J. (1997). Crystal structure of the cytochrome bc_1 complex from bovine heart mitochondria. *Science* **277**, 60-66.
7. Zhang, Z., *et al.*, & Kim., S.-H. (1998). Electron transfer by domain movement in cytochrome bc_1. *Nature* **392**, 677-684.
8. Iwata, S., *et al.*, & Jap, B.K. (1998). Complete structure of the 11-subunit bovine mitochondrial cytochrome bc_1 complex. *Science* **281**, 64-71.
9. Iwata, S., Saynovits, M., Link, T.A. & Michel, H. (1996). Structure of a water soluble fragment of the 'Rieske' iron–sulfur protein of the bovine heart mitochondrial cytochrome bc_1 complex determined by MAD phasing at 1.5 Å resolution. *Structure* **4**, 567-579.
10. Mitchell, P. (1976). Possible molecular mechanisms of the protonmotive function of cytochrome systems. *J. Theor. Biol.* **62**, 327-367.
11. Crofts, A.R. (1985). The mechanism of ubiquinol:cytochrome c oxidoreductases of mitochondria and of *Rhodopseudomonas sphaeroides*. In *The Enzymes of Biological Membranes.* (Martonosi A.N., ed.), pp. 347-382, New York, Plenum Publishing Corporation.
12. Kim H., *et al.*, & Deisenhofer, J. (1998). Inhibitor binding changes domain mobility in the iron–sulfur protein of the mitochondrial bc_1 complex from bovine heart. *Proc. Natl Acad. Sci. USA* **95**, 8026-8033
13. Brasseur, G., Saribas, A.S. & Daldal, F. (1996). A compilation of mutations located in the cytochrome *b* subunit of the bacterial and mitochondrial bc_1 complex. *Biochim. Biophys. Acta* **1275**, 61-69.
14. Ostermeier, C. Iwata, S., Ludwig, B. & Michel, H. (1995). Fv fragment-mediated crystallization of the membrane protein bacterial cytochrome *c* oxidase. *Nat. Struct. Biol.* **2**, 842-846.
15. Iwata, S., Ostermeier, C., Ludwig, B. & Michel, H. (1995). Structure at 2.8 Å resolution of cytochrome *c* oxidase from *Paracoccus denitrificans. Nature* **376**, 660-669.
16. Ostermeier, C., Harrenga, A., Ermler, U. & Michel, H. (1997). Structure at 2.7 Å resolution of the *Paracoccus denitrificans* two-subunit cytochrome c oxidase complexed with an antibody Fv fragment. *Proc. Natl Acad. Sci. USA.* **94**, 10547-10553.
17. Fu, W., Japa, S.& Beattie, D.S. (1990). Import of the iron–sulfur protein of the cytochrome bc_1 complex into yeast mitochondria. *J. Biol. Chem.* **265**, 16541-16547.
18. Boumans, H., Berden, J.A. & Grivell, L.A. (1997). The role of subunit VIII in the structural stability of the bc_1 complex from *Saccharomyces cerevisiae* studied using hybrid complexes. *Eur. J. Biochem.*

249, 762-769.
19. Stonehuerner, J., *et al.,* & Yu, C.-A (1991). Identification of the binding site on cytochrome c_1–*c*. *J. Biol. Chem.* **260**, 5392-5398.
20. Kim, C.H. & King, T.E. (1983). A mitochondrial protein essential for the formation of the cytochrome c_1–*c* complex. Isolation, purification, and properties. *J. Biol. Chem.* **258**, 13543-13551.
21. Kim, C.H., Balny, C. & King (1987). Role of the hinge protein in the electron transfer between cardiac cytochrome c1 and c. Equilibrium constants and kinetic probes. *J. Biol. Chem.* **262**, 8103-8108.
22. Schmitt, M.E. & Trumpower, B.L. (1990). Subunit 6 regulates half of-the-sites reactivity of the dimeric cytochrome bc_1 complex in *Saccharomyces cerevisiae*. *J. Biol. Chem.* **265**, 17005-17011.
23. Rawlings N.D. & Barrett, A.J. (1991). Homologues of insulinase, a new superfamily of metallopeptidases. *Biochem. J.* **275**, 389-391.
24. Yang, M., Jensen, R.E., Yaffe, M. P., Oppliger, W. & Schatz, G. (1988). Import of proteins into yeast mitochondria: the purified matrix processing protease contains two subunits which are encoded by nuclear MAS1 and MAS2 genes. *EMBO J.* **7**, 3857-3862.
25. Braun, H.-P., Emmermann, M., Kruft, V. & Schmitz, U.K. (1992). The general mitochondrial processing peptidase from potato is an integral part of cytochrome *c* reductase of the respiratory chain. *EMBO J.* **11**, 3219-3227.
26. Schulte, U., Arretz, M., Schneider, H., Tropschug, M., Wachter, E., Neupert, W. & Weiss, H. (1989). A family of mitochondrial proteins involved in bioenergetics and biogenesis. *Nature* **339**, 147-149.
27. Deng, K., *et al*., & Yu, C.-A. (1998). Activation of a matrix processing peptidase from the crystalline cytochrome bc_1 complex of bovine heart mitochondria. *J. Biol. Chem.* **273**, 20752-20757.
28. Tzagaloff, A., Wu, M. & Crivellone, M. (1986). Assembly of the mitochondrial membrane system. Characterization of COR1, the structural gene for the 44-kilodalton core protein of yeast coenzyme QH2-cytochrome c reductase. *J. Biol. Chem.* **261**, 17163-17169.
29. Oudshoorn, P., Van Steeg, H., Swinkels, B.,W., Schoppink, P. & Grivell, L. A. (1987) Subunit II of the genes encoding the 40 kD subunit II or the 17 kD subunit VI on the steady-state kinetics of yeast ubiquinol-cytochrome-*c* oxidoreductase. Nucleotide sequence of the gene and features of the protein. *Eur. J. Biochem.* **163**, 97-103.
30. Braun, H.-P. & Schmitz, U.K. (1995). Are the 'core' proteins of the mitochondrial bc_1 complex evolutionary relics of a processing protease? *Trends Biochem. Sci.* **20**, 171-174.
31. di Rago, J.-P., Sohm, F., Boccia, C., Dujardin, G., Trumpower, B.L. & Slonimski, P. P. (1997). A point mutation in the mitochondrial cytochrome *b* gene obviates the requirement for the nuclear encoded core protein 2 subunit in the cytochrome bc_1 complex in *Saccharomyces cerevisiae*. *J. Biol. Chem.* **272**, 4699-4704.
32. Lancaster, C.R.D. & Michel, H. (1997). The coupling of light-induced electron transfer and proton uptake as derived from crystal structures of reaction centres from *Rhodopseudomonas viridis* modified at the binding site of the secondary quinone, QB. *Structure* **5**, 1339-1359.
33. Link, T.A. (1997). The role of the 'Rieske' iron sulfur protein in the hydroquinone oxidation (QP) site of the cytochrome bc_1 complex. *FEBS Lett.* **412**, 257-264.
34. Crofts, A.R., *et al.,* & Berry, E.A. (1999). Pathways for proton release during ubihydroquinone oxidation by the bc_1 complex. *Proc. Natl Acad. Sci. USA* **96**, 10021-10026.
35. Degli Esposti M., De Vries, S., Crimi, M., Ghelli, A., Patarnello, T. & Meyer, A. (1993). Mitochondrial cytochrome *b*: evolution and structure of the protein. *Biochim. Biophys. Acta* **1143**, 243 -271
36. Berry, E.A., Huang, L. & DeRose, V.J. (1991). Ubiquinol-cytochrome *c* oxidoreductase of higher plants. *J. Biol. Chem.* **266**, 9064-9077.
37. Kleymann, G., Ostermeier, C., Ludwig, B., Skerra, A., & Michel, H. (1995). Engineered Fv fragments as a tool for the one-step purification of integral multisubunit membrane protein complexes. *Bio/Technol.* **13**, 155-160.
38. Otwinowski, Z.(1993). Oscillation data reduction program. In Proceedings of the CCP4 Study Weekend: Data Collection and Processing. (Sawyer, L., Isaacs, N. & Bailey, S., eds), pp.56-62, SERC Daresbury Laboratory, Warrington, UK.
39. Minor, W. (1993). XDISPLAYF Program. Purdue University.
40. Collaborative Computer Project No. 4. (1994). The CCP4 suit: programs for protein crystallography. *Acta Crystallogr. D* **50**, 760-763.
41. Brünger, A.T. (1992). X-PLOR, Version 3.1: a system for X-ray crystallography and NMR. Yale University Press, New Haven, CT.
42. Brünger, A.T. (1990). Extension of molecular replacement: a new search strategy based on Patterson correlation refinement. *Acta Crystallog. A* **38**, 46-57.
43. Cowtan, K. (1994). 'dm': an automated procedure for phase improvement by density modification. *Joint CCP4 and ESF-EACBM Newsletter on Protein Crystallography* **31**, 34-38.
44. Lamzin, V.S. and Wilson, K.S. (1993). Automated refinement of protein models. *Acta Crystallogr. D* **49**, 129-149.
45. McRee, D.E. (1993) *Practical Protein Crystallography,* Academic Press Inc.
46. Jones, A., Zou, J.-Y., Cowan, S., & Kjeldgaard,M.(1991). Improved methods for building protein models in electron-density maps and the location of error in these models. *Acta Crystallogr. A* **47**, 110-119.
47. Brünger, A.T., *et al.* & Warren, G.L. (1998). Crystallographic and NMR system: a new software suite of macromolecular structure determination. *Acta Crystallogr. D* **54**, 905-921.
48. Brünger, A.T. (1992). Free R value: a novel statistical quantity for assessing the accuracy of crystal structures. *Nature* **335**, 472-474.
49. Costanzo, M.C., *et al.*, & Garrels, J.I. (2000). The yeast proteome Database (YPD) and *Caenorhabditis elegans* proteome database (WormPD): comprehensive resources for the organization and comparison of model organism protein information. *Nucleic Acids Res.* **28**, 73-76.
50. Holm, L. & Sander, C. (1996). Mapping the protein universe. *Science* **273**, 595-602.
51. Humphrey, W.F., Dalke, A., & Schulten, K. (1996) VMD: Visual Molecular Dynamics. *J. Mol. Graph.* **14**, 33-8, 27-8.
52. Ippolito, J.A., Alexander, R.S. & Christianson, D.W. (1990). Hydrogen bond stereochemistry in protein structure and function. *J. Mol. Biol.* **215**, 457-471.